Atmos. Chem. Phys., 10, 6993–7008, 2010
www.atmos-chem-phys.net/10/6993/2010/
doi:10.5194/acp-10-6993-2010

Atmospheric Chemistry and Physics

Oxidative capacity of the Mexico City atmosphere – Part 2: A RO_x radical cycling perspective

P. M. Sheehy[1,2], **R. Volkamer**[1,3,4], **L. T. Molina**[1,2], **and M. J. Molina**[1,3]

[1]Massachusetts Institute of Technology, Cambridge, MA, USA
[2]Molina Center for Energy & the Environment, La Jolla, CA, USA
[3]University of California at San Diego, La Jolla, CA, USA
[4]University of Colorado at Boulder and CIRES, Boulder, CO, USA

Received: 20 December 2007 – Published in Atmos. Chem. Phys. Discuss.: 17 March 2008
Revised: 12 July 2010 – Accepted: 14 July 2010 – Published: 30 July 2010

Abstract. A box model using measurements from the Mexico City Metropolitan Area study in the spring of 2003 (MCMA-2003) is presented to study oxidative capacity (our ability to predict OH radicals) and RO_x (RO_x=OH+HO_2+RO_2+RO) radical cycling in a polluted (i.e., very high NO_x=NO+NO_2) atmosphere. Model simulations were performed using the Master Chemical Mechanism (MCMv3.1) constrained with 10 min averaged measurements of major radical sources (i.e., HCHO, HONO, O_3, CHOCHO, etc.), radical sink precursors (i.e., NO, NO_2, SO_2, CO, and 102 volatile organic compounds (VOC)), meteorological parameters (temperature, pressure, water vapor concentration, dilution), and photolysis frequencies.

Modeled HO_x (=OH+HO_2) concentrations compare favorably with measured concentrations for most of the day; however, the model under-predicts the concentrations of radicals in the early morning. This "missing reactivity" is highest during peak photochemical activity, and is least visible in a direct comparison of HO_x radical concentrations. We conclude that the most likely scenario to reconcile model predictions with observations is the existence of a currently unidentified additional source for RO_2 radicals, in combination with an additional sink for HO_2 radicals that does not form OH. The true uncertainty due to "missing reactivity" is apparent in parameters like chain length. We present a first attempt to calculate chain length rigorously i.e., we define two parameters that account for atmospheric complexity, and are based on (1) radical initiation, n(OH), and (2) radical termination, ω. We find very high values of n(OH) in the early morning are incompatible with our current understanding of RO_x termination routes. We also observe missing reactivity in the rate of ozone production ($P(O_3)$). For example, the integral amount of ozone produced could be under-predicted by a factor of two. We argue that this uncertainty is partly accounted for in lumped chemical codes that are optimized to predict ozone concentrations; however, these codes do not reflect the true uncertainty in oxidative capacity that is relevant to other aspects of air quality management, such as the formation of secondary organic aerosol (SOA). Our analysis highlights that apart from uncertainties in emissions, and meteorology, there is an additional major uncertainty in chemical mechanisms that affects our ability to predict ozone and SOA formation with confidence.

1 Introduction

Implementing robust air pollution control strategies as part of effective air quality management requires a detailed understanding of the oxidative capacity of the atmosphere: the oxidation of volatile organic compounds (VOC) initiated by the hydroxyl radical (OH) starts radical cycling via HO_x and NO_x chemistry in the troposphere that drives a variety of chemical processes, including ozone formation and secondary organic aerosol (SOA) formation. In an urban area, the complexity of the tropospheric chemistry is increased by anthropogenic emissions, which requires sophisticated

Correspondence to: R. Volkamer
(rainer.volkamer@colorado.edu)

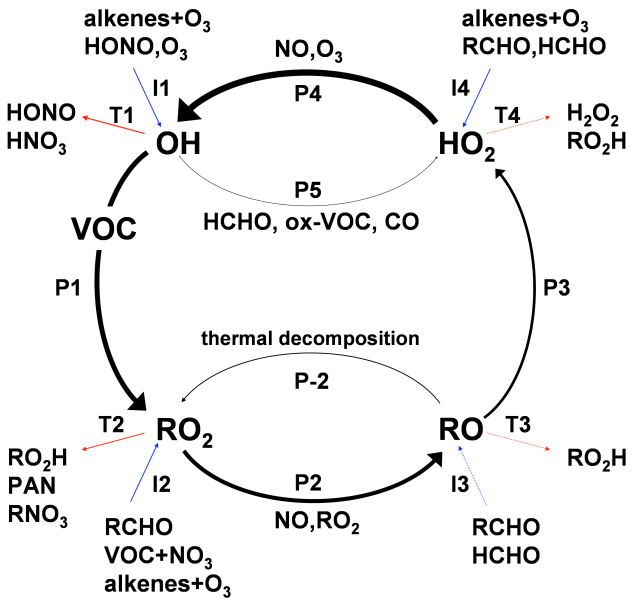

Fig. 1. The schematic of RO_x cycling in MCMA is shown. Only the predominant species involved in radical sources, sinks, and cycling are shown. Radical pathways are labeled as initiation (I), propagation (P), or termination (T), and assigned a number for cross-referencing in Table S1 (see Supplemental Information). The thickness of each arrow corresponds to the magnitude of the radical pathway, as determined in the HO_x-unconstrained scenario.

chemical models to formulate effective control and mitigation strategies.

The oxidation of VOC (see Fig. 1) generates organic peroxyl radicals, RO_2, which can react with nitric oxide (NO), NO_3, and other RO_2 to form the analog alkoxy radical (RO), and nitrogen dioxide (NO_2). The alkoxy radical reacts in the presence of oxygen to generate the hydroperoxyl radical, HO_2, which will readily react with NO to generate recycled OH and NO_2. The conversion of NO to NO_2 via RO_x cycling in the troposphere followed by NO_2 photolysis is key to understanding ozone formation. Studying the reactive processes of these radicals is essential to understanding the general oxidative capacity of the atmosphere.

Radical initiation – the breakdown of a closed shell species yielding a new radical – plays an important role in tropospheric chemistry, as it starts the processes that form secondary pollutants; however, radical cycling – the amplification of new radicals in the RO_x-NO_x cycle – dominates in polluted atmospheres e.g., Mexico City Metropolitan Area (MCMA), where NO_x concentrations are high enough so that radical propagation reaction rates dominate over radical terminiation rates and can be up to an order of magnitude greater than radical source terms. In a companion paper Volkamer et al. (2010) quantify new radical production ($P(HO_x)$) in the MCMA and on average, 20% of radical production is attributable to the breakdown of closed shell species, while 80% is due to radical cycling. As such, it is important that we understand radical cycling (and recycling), in addition to radical sources.

Direct detection of OH and HO_2 is difficult because they are both highly reactive and are present at low concentrations. Although an increasing number of studies combine OH and HO_2 measurements and modeling, only a few field campaigns included HO_x measurements in a polluted urban or semi-urban atmosphere. Measurements of HO_x in an urban atmosphere have been made in London (Abram et al., 2000) and Birmingham, UK (Heard et al., 2004); Los Angeles, CA (George et al., 1999); Nashville, TN (Martinez et al., 2003); Houston, TX (Martinez et al., 2002); New York, NY (Ren et al., 2003); near Berlin, Germany (Platt et al., 2002)[1]; at Birmingham near London (Emmerson et al., 2007); and more recently in Mexico City (Shirley et al., 2006; Dusanter et al., 2009). The study described here is characterized by a very polluted airmass in the MCMA with elevated levels of NO_x (with campaign median concentrations ranging from 8–134 ppb throughout the day).

The focus of this work is similar to that of Emmerson et al. (2007), and includes comparisons between predicted and measured values of OH and HO_2 to RO_x, and a detailed analysis of the impact of radical cycling on the oxidative capacity of the urban troposphere. Our work differs in that we are dealing with extraordinarily high NO_x concentrations and VOC loadings, and explore the effects of these unique characteristics of the airmass on radical initiation (Volkamer et al., 2010) and the amplification of these new radicals due to cycling. The extensive amount of data collected during the MCMA-2003 campaign (Molina et al., 2007) and recent improvements to the MCM (Bloss et al., 2005a,b) afford an excellent opportunity to explore a variety of questions related to RO_x chemistry. In general, predicted HO_x radical concentrations are lower than measured concentrations, and defined here as "missing reactivity". The term "missing reactivity" is used because the lower-than-measured concentrations of radicals leads to lower levels of reactivity in the RO_x radical cycling. This in turn affects reactive processes such as ozone and SOA formation. This "missing reactivity" is discussed in greater detail below, and leads to an analysis of the mechanism with regard to RO_x cycling. Model scenarios are varied with regard to HO_x to elucidate the effects of "missing reactivity" on VOC oxidation and photochemical ozone production in the MCMA.

We use a near-explicit chemical mechanism to evaluate the impacts of the "missing reactivity" via quantitative measures such as chain length and ozone production. Chain length is a measure of the number of times that OH goes through the RO_x cycle before a termination reaction. Whereas Part 1 of this study (Volkamer et al., 2010) focuses on radical

[1]This refers to a semi-rural/urban site near Berlin, Germany. It is important to note that the highest levels of observed NO were limited to a few ppb_v and that there were strong biogenic influences.

initiation, this work focuses on radical propagation or recycling. The calculation of chain length is dependent on an implicit knowledge of branching ratios[2] within the chemical mechanism. Ozone production is another quantitative parameter used to understand "missing reactivity". The variables used to calculate ozone production are well constrained by measurements, which enables a useful comparison to the value calculated using the modeled values.

2 The mechanism and the model

The work presented here was performed using the latest version of the Master Chemical Mechanism (MCMv3.1) (Bloss et al., 2005a,b). This version of the MCM includes the degradation kinetics and oxidation schemes of 135 VOC, based on mechanisms described by Jenkin et al. (1997) and Saunders et al. (2003). The updated version includes an improved understanding of aromatic schemes using results from recent laboratory studies (e.g., Olariu et al., 2000; Olariu, 2001; Volkamer et al., 2001; Bethel et al., 2001; Martin et al., 2002; Volkamer et al., 2002). The MCMv3.1 is well suited over a wide range of NO_x and VOC conditions because it explicitly represents the sources and sinks of OH, HO_2, and RO_2 radicals, rather than lumping them. The near-explicit code enables the user to account for individual reactive pathways, which is ideally suited to study RO_x radical cycling. We used the FACSIMILE (Curtis and Sweetenham, 1987) software package as our numerical integrator for the box model.

The model calculations were performed on a 24-h basis, and were initialized every 10-min with the constrained input parameters listed below. The model is constrained for the following major species, including measurement uncertainties: NO (±15%), NO_2 (±20%), HONO (±10%), O_3 (±15%), SO_2 (±20%), and CO (±15%). The model is also constrained for 100 VOC (see Supplemental Material), temperature, pressure, water vapor concentration, J-values, and dilution in both the horizontal and vertical fields. Photolysis frequencies were measured by spectroradiometry, and the dilution parameter used is described in Part 1 (Volkamer et al., 2010).

The following modeling scenarios, in terms of constraints, were used to study HO_x chemistry in the MCMA, including estimated model uncertainties for each case:

– HO_x-unconstrained: The model was constrained for species including NO, NO_2, HONO, O_3, SO_2, CO, 100 VOC, temperature pressure, water vapor concentration, J-values, and dilution in both the horizontal and vertical fields. In this case, we report model uncertainties for OH and HO_2 of ±55% and ±70%, respectively.

– OH-constrained: in addition to the parameters listed in the HO_x-unconstrained case, a campaign median diurnal profile of OH is used to constrain the mechanism. In this case, we estimate an uncertainty of ±60% for HO_2.

– HO_2-constrained: in addition to the parameters listed in the HO_x-unconstrained case, a campaign median diurnal profile of HO_2 is used to constrain the mechanism. In this case, we estimate an uncertainty of ±45% for OH.

  The OH- and HO_2-constrained cases are a means to explore linear and non-linear feedbacks related to RO_x radical sources, propagation, and termination, most notably by predicting the unconstrained HO_x radical.

– HO_x-constrained: in addition to the parameters listed in the HO_x-unconstrained case, we used a campaign median diurnal profile of both OH and HO_2, from Shirley et al. (2006) to constrain the mechanism in addition to the parameters described above. The HO_x measurements were increased by a factor of 1.3 in accordance with recommended changes to previously reported measurements (W. H. Brune, personal communication, 2007). Shirley et al. (2006) report a measurement uncertainty of ±32%.

In each case, model uncertainties were determined based on a) the experimental uncertainties of the dominant reaction rate constants for initiation (e.g., HONO photolysis), propagation (e.g., HO_2+NO), and termination (e.g., peroxide or nitrate formation) routes for each HO_x radical and b) measurement uncertainties for species constrained in the model.

Note that the HO_x-unconstrained model, the OH-constrained model, and the HO_2 constrained model yield a balanced model i.e., the radical termination, propagation, and initiation pathways for a radical are net zero. For instance, in a balanced model, the pathways for OH shown in Fig. 1 will yield the following: I1+P4=T1+P1+P5.

Apart from varying the constraints imposed on the model, we ran the model for a) individual days, b) campaign median concentration time profiles, and c) campaign average concentration time profiles in both unconstrained and constrained scenarios. The model was run for 18 days, 9–24 April 2003. We observed differences between concentration time profiles on a median and average basis, most notably at night. The results presented here focus exclusively on individual days and a median model, as night-time concentrations of NO – an important determinant in radical recycling rates (HO_2/RO_2+NO) – are up to 6 times higher on an average basis as compared to a median basis. As such, we consider the campaign average NO concentrations as statistical forcing rather than a realistic representation of the airmass and minimize this forcing by using median profiles.

[2] In this context, we use the term "branching ratio" to refer to the ratio of radical fluxes of the multiple reaction pathways of a RO_x radical. This is not to be confused with the term branching ratio used in chain reaction theory for combustion kinetics.

Note that all concentrations, unless otherwise mentioned, are reported in parts per billion by volume (ppb_v), and all times are reported as Central Standard Time (CST i.e., Coordinated Universal Time minus 6 (UTC−6)).

The model was constrained for 21 alkanes, 19 alkenes, 16 aromatics, and 23 oxygenated VOC, which includes alcohols, aldehydes, ketones, esters, ethers, and organic acids. The uncertainty for each parameter is a combination of measurement error, day-to-day variability, and the scaling methodology employed (as appropriate). See the discussion in the Supplemental Material for a more detailed description of the measurements, methodologies, and uncertainties for each of the constrained species.

We introduced a dilution parameter to represent physical transport of chemical species out of the MCMA. The reactive species in the model were diluted using a combination of two approaches: 1) using traffic counts and measured concentrations of CO (traffic-CO) to generate a proxy for the rising planetary boundary layer (PBL), and 2) by matching predicted photochemical HCHO with observations. If only the traffic-CO approach is used, then uncharacteristic chemical accumulation is observed. The increased dilution as a result of the HCHO modeling eliminates this unrepresentative accumulation of secondary products (i.e., oxidized volatile organic compounds, OVOC). For a more detailed discussion of the methodology employed to constrain the model for dilution, see Part 1 (Volkamer et al., 2010).

The photolysis frequencies for O_3 (J_{O_3}, ±25%), NO_2 (J_{NO_2}, ±15%), HCHO (J_{HCHO}, ±15%), CH_3CHO (J_{CH_3CHO},±15%), and HONO (J_{HONO},±15%) are constrained by measurements (Volkamer et al., 2005). The values for J_{HONO} have been multiplied by 1.43 to match recent absolute measurements made by Wall et al. (2006) consistent with results presented in Volkamer et al. (2010). The measured downwelling portion of each J-value was multiplied by 1.08 to account for surface albedo corrections. The code calculates photolysis rates solely as a function of solar zenith angle, which does not account for cloud coverage, scattering in the atmosphere, and the albedo of the earth's surface. As such, the photolysis rates are corrected using a factor that is based on the average difference between the calculated and measured values for J_{NO_2}. Calculations were initially performed using clear sky conditions at a latitude of 19°21′32″ N and a longitude of 99°4′25″ W.

2.1 OH reactivity: first order loss of OH

For each of the modeling scenarios described previously, with the exception of the HO_x-constrained scenario, OH loss is equal to OH production within τ_{OH} <0.1 s, i.e., OH is in steady state. The modeled and median measured OH reactivity – the pseudo first order rate loss of OH – are shown in the bottom panel of Fig. 2; the total OH reactivity predicted by the model is about 110 s^{-1} during morning rush hour and a value of roughly 20–25 s^{-1} during the day and between 45–50 s^{-1} at night. These values are consistent with those measured by Shirley et al. (2006); however, there is a significant difference between measured and modeled values from 05:00–07:00, when NO_x values are highest. The uncertainty in the total OH loss measurement is highest under high NO_x conditions (Shirley et al., 2006). The degree of constraint imposed on the mechanism by inputs in terms of OH reactivity is shown in the upper panel of Fig. 2. Most notably, the fraction of OH reactivity due to reaction with unconstrained parameters linearly increases in the morning around 08:00 until 12:00. This increase is roughly 1 h after the onset of photochemical processing and due to the oxidation of primary VOC, resulting in the formation of secondary products. The formation of secondary products and their subsequent oxidation results in an increase of unconstrained OH loss of roughly 5% per hour, reaching a maximum of 25%. The decrease in the fraction of OH loss from unconstrained parameters around 12:00 reflects the venting of the MCMA, is consistent with an observed decrease in new OH radical production (Volkamer et al., 2010), and reflects the dilution implemented in the code (see Volkamer et al. (2010) for details).

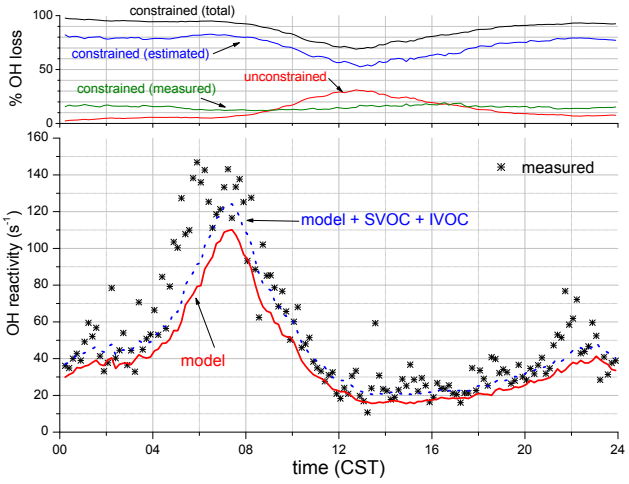

Fig. 2. The bottom panel shows the median measured (stars) and modeled (red solid line) OH loss; we also include a plot of modeled OH loss augmented with an estimated OH loss due to primary organic aerosol (POA) vapors (SVOC+IVOC) as parameterized by Robinson et al. (2007). Note the under-estimation of OH loss by the model between 05:00–07:00. In the upper panel, the profile of OH loss in the model is separated into constrained parameters (black line) and unconstrained parameters (red line). The constrained parameters are further distinguished as parameters constrained by measurements (green line) and those that were estimated (blue line) based on emissions information in the literature. Constrained parameters account for some 75–98% of total modeled OH loss throughout the day.

3 Results and discussion

3.1 Missing OH reactivity

Recent findings indicate that primary organic aerosol (POA) upon dilution from the tailpipe of a car to atmospheric conditions may act as a source of semivolatile hydrocarbons in urban air, so-called semi-volatile organic compounds (SVOC) and intermediate volatility organic compounds (IVOC) (Donahue et al., 2006; Robinson et al., 2007). SVOC and IVOC make a significant contribution to SOA formation (Dzepina et al., 2009). The chemical identity of these hydrocarbons is unclear, and, as such, SVOC and IVOC are not represented in MCM. These species could be relevant to SOA formation (Robinson et al., 2007) and possibly ozone production. We estimate here for the first time the possible contribution of SVOC and IVOC to OH reactivity to assess whether the gap between modeled and measured reactivity can be attributed to these species. We calculated the OH reactivity of SVOC and IVOC by estimating the amount of each in the gas phase using POA measurements (Salcedo et al., 2006): SVOC+IVOC=4·POA+7.5·POA. Here, we parameterized the data from Fig. 1a in Robinson et al. (2007) to account for the effects of variable partitioning depending on POA partitioning mass. We used a molecular weight of $250\,g\,mol^{-1}$ (corresponding to a C_{18} alkane), suggested by Robinson et al. (2007), to convert $\mu g\,m^{-3}$ to units of molec cm^{-3}. Using this concentration, and a generic rate constant for reaction with OH radicals of $4\times10^{-11}\,cm^3\,molec^{-1}\,s^{-1}$ reported by Robinson et al. (2007), we calculate the corresponding OH loss rate. The results are plotted as an overlay in Fig. 2. Using this methodology, we observe a modest increase of $4–14\,s^{-1}$ of OH reactivity (about 10% of the measured value). The existence of SVOC and IVOC is consistent with the observation of a gap in OH reactivity, though insufficient to obtain closure. The OH reactivity in our model is about 10–20% too low. The largest differences tend to be observed between 04:00–06:00, and also in the afternoon (12:00–16:00). Notably, Lewis et al. (2000) identified an additional mechanism for OH loss in terms of volatile carbon in the range of C_6 to C_{14} as oxygenated aromatic and aliphatic molecules. These molecules are difficult to quantify with the measurement techniques used during MCMA-2003, and they appear to be only partially captured by our model-predicted OVOCs, and estimates of SVOC/IVOC. Notably, the portion of unaccounted OH reactivity in our model is relatively small and we do not observe an over-prediction of OH radicals in the afternoon as has been noted in previous studies (Lewis et al., 2000; Carslaw et al., 1999). Future studies will need to demonstrate whether the parameterization of SVOC and IVOC from laboratory generated POA provide for a meaningful extrapolation to the atmosphere, and whether additional unmeasured compounds could cause additional OH loss. It appears, however, from this analysis that SVOC and IVOC, in addition to their role as SOA precursors, also make a sufficiently large contribution to OH reactivity to be potentially relevant to O_3 formation.

3.2 HO_x: measured vs. modeled

The HO_x-unconstrained model accurately predicts the diurnal profile of both OH and HO_2, as shown in Fig. 3a, c. When compared to a lower limit of measured OH values[3], the model predicts OH concentrations within measured and modeled uncertainties for the day with the exception of about 05:30 to 06:30 (Fig. 3a). In the early morning, between 06:00–07:00 (i.e., rush hour), the model underpredicts OH radicals by about a factor of 3–4. Similarly, a consistent under-prediction is observed in the evening after 18:00, though slightly less than in the morning. Between 07:30–16:00, the model and the measurements are in excellent agreement, with the ratio of measured-to-modeled concentrations varying between 0.93 and 1.35 i.e., within error bars of the measurements and the model.

The model under-predicts the concentration of HO_2 for the entire day, and most notably between midnight and 10:00. The measured-to-modeled ratios are consistently between 3–10 before 07:00. The predicted concentrations do not fall within the measurement and modeled uncertainty until around 10:00. The model predicts HO_2 concentrations within modeled and measured uncertainties between 10:00 and 18:30. Thereafter, the ratio of measured-to-modeled concentrations starts increasing and varies between 5–12 for the remainder of the day.

The median concentrations of predicted OH and HO_2 from individual day modeling show good agreement with the predicted OH and HO_2 from the HO_x-unconstrained model of campaign median concentration inputs of HO_x sources and sinks (not shown). A linear regression of individual day OH and HO_2 modeled predictions versus measured values yields the following relationships:

$[OH]_{model} = 0.73\cdot[OH]_{meas}+0.02$ ppt, R^2=0.98, and

$[HO_2]_{model} = 0.74\cdot[HO_2]_{meas}-2.79$ ppt, R^2=0.96.

Despite what appears to be an excellent correlation ($R^2>0.95$) between measured and modeled values, a more thorough analysis shows these results belie the lack of radicals at high concentrations of NO_x. For both OH and HO_2, the measured-to-modeled regression relationship is predominantly determined by the higher concentrations in the afternoon. As such, the linear regression is skewed in favor of times when the model more accurately predicts HO_x concentrations (which, is also at low NO_x conditions).

[3]The lower limit is based on a $0.01\,ppt_v$ statistical offset. We found that there was improved agreement between measured and modeled OH concentrations based on overlap of error bars, in addition to better agreement in the comparison of measured and modeled HONO concentrations using the lower limit of OH. See Volkamer et al. (2010) for a more detailed discussion

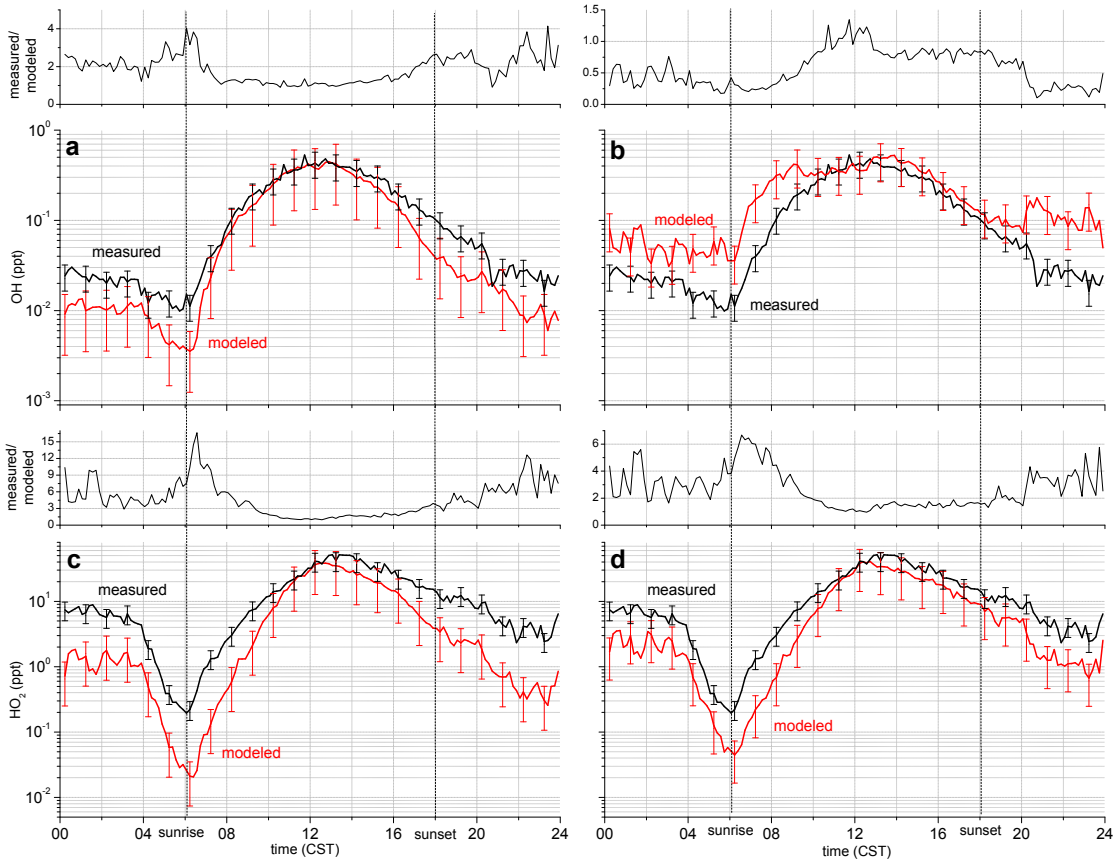

Fig. 3. Measured (black) and modeled (red) diurnal concentrations of HO_x are shown for each of the three balanced model cases: **(a)** OH, HO_x-unconstrained, **(b)** OH, HO_2-constrained, **(c)** HO_2, HO_x-unconstrained, and **(d)** HO_2, OH-constrained. In the upper panel of each graph, the measured-to-modeled ratios are also shown. Note that for the top panels of OH, A and B, "measured" refers to values reported by Shirley et al. (2006) multiplied by 1.3 and include a 0.01 ppt offset subtracted from the measured values as discussed in the text and in Volkamer et al. (2010).

When the model is constrained for HO_2 (Fig. 3b), it is unable to predict the diurnal profile of OH. As a result of the HO_2 forcing, the model over-predicts the concentration of OH for the majority of the day, most notably in the morning 04:00–10:00, and at night, 19:00–24:00. The overprediction of OH from the HO_2-constrained model is partly compensated by the fact that our pseudo-first-order OH loss rate is most underestimated during this part of the day (see Fig. 2). The HO_2 constrained prediction of OH would be in better agreement with the observations if this missing OH loss was accounted for. Despite this limitation, we do observe overlap in the observed and predicted concentrations during much of the day, 10:00–18:00. The distorted diurnal profile of OH and the over-prediction of the concentration reflects the strong coupling between HO_2 and OH via NO.

The OH forcing (Fig. 3d) affects modeled HO_2 concentrations less directly, particularly because it involves the entire RO_x cycle; however, the effects of the OH forcing are significant. Most notably, from midnight to 06:00 and again from 18:00–24:00, the measured and modeled HO_2 are in much better agreement. Conversely, the model still drastically under-predicts the concentrations of HO_2 shortly after sunrise until 09:30. This suggests that the gas-phase mechanism is lacking a HO_2 (or RO_2) production term.

The exercise of forcing OH and HO_2 concentrations in the mechanism is valuable, as it can help elucidate shortcomings in the mechanism. The HO_2-forcing suggests that the gas-phase mechanism – particularly under high NO_x conditions – lacks either a significant HO_2 source that does not form OH or an HO_2 source and OH sink. However, a large missing gas phase OH sink appears unlikely, because the modeled predictions of OH show good agreement with measurements in the HO_x-unconstrained case, and because of high uncertainty in the OH loss measurements. This is inconsistent with the relatively small differences between measured and modeled OH loss (Fig. 2). Similarly, the modeled OH in the HO_x-unconstrained case is generally under-predicted, which does not lend support to the argument that the mechanism has a missing sink for OH.

3.3 HO_2/OH vs. NO

Apart from absolute HO_x concentrations, the ratio of HO_2 to OH as a function of NO is a useful relationship to test our understanding of HO_x cycling (Fig. 4). We compare measured and modeled HO_x ratios vs. NO on both a campaign median basis and an individual day basis. For the sake of comparison, we binned OH, HO_2, and NO values based on 10 different ranges of NO concentrations. The error bars show the uncertainty of the HO_x ratio, calculated based on the uncertainty of modeled OH and HO_2 concentrations.

We observe a similar relationship between the HO_2/OH ratio and NO for both the measured and modeled values; however, there are significant differences at high NO. The modeled HO_2/OH ratio is lower than the measured ratios by roughly a factor of 4 at NO concentrations of 100 ppb. The difference narrows to a factor of 2–3 between NO concentrations of 10–100 ppb, and is $\leq$2 for NO concentrations between 1–10 ppb. The larger differences between modeled and measured HO_2/OH ratios at high NO occurs in the morning and at night, when the model most drastically underestimates the concentrations of HO_2.

The "missing reactivity" noted previously is also evident in the comparison of the NO dependence of measured and predicted HO_2/OH ratios. The measured HO_x ratio has a shallower slope with respect to NO than the modeled ratio does. The slope of the graphs in Fig. 4 yield the NO power dependence. We expect a dependence of between 1 to 2 (Shirley et al., 2006); however, the measured values of the HO_2/OH vary as NO to the power of 0.36, and the modeled values vary as NO to the power of 0.64, nearly a factor of 2 increase. The lower-than-expected NO power dependence is tentatively attributed to more efficient HO_x cycling in VOC chemistry and is consistent with laboratory observations (Bloss et al., 2005a,b).

The HO_2/OH ratio vs. NO relationship is also useful in determining the effects of using median diurnal profiles from campaign data for modeling. Legitimate concerns exist regarding conclusions drawn from the use of average or median diurnal profiles of radical sources and sinks, particularly because the characteristics of fast HO_x-NO_x chemistry may not be captured. To test our use of campaign median data and day-to-day variability thereof, we predicted HO_x concentrations for a "high NO_x" day (11 April, NO_{max} =220 ppb) and a "low NO_x" day (18 April, NO_{max} =24 ppb). The modeled HO_2/OH results are also shown in Fig. 4; the individual day results – for both the measurements and the modeling – show good agreement with the campaign median results, confirming the utility of modeling on a campaign median basis.

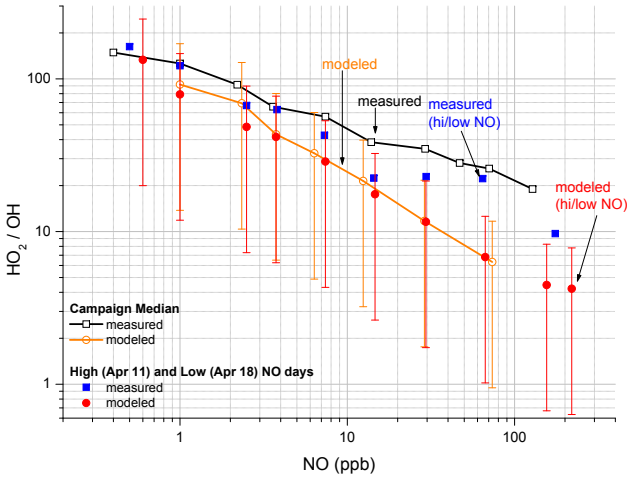

Fig. 4. The HO_2/OH ratio as a function of NO. For graphical purposes, all of the HO_x ratios are binned based on ranges of NO concentrations. We used the following bins: 0–1 ppb, 1–2 ppb, 2–3 ppb, 3–5 ppb, 5–10 ppb, 10–20 ppb, 20–40 ppb, 40–100 ppb, and 100–200 ppb. Each circle or square represents the median of each NO concentration bin. The predicted values from the model on a campaign median basis are shown as the orange line with open circles, whereas the median measured values from the entire campaign are shown as a black line with open squares. The closed red circles and closed blue squares are the modeled and measured HO_x ratios, respectively, for the high and low NO days, 11 and 18 April. Note that the lines are *not* a fit through the symbols, but rather connect the symbols to help guide the eye.

3.4 Predicting RO_2

Organic peroxyl radicals play a major role in atmospheric processes, most notably in its reaction with NO yielding NO_2, adding to O_3 production. Unfortunately, ambient measurements of RO_2 are difficult, and unavailable from MCMA-2003. As such, we use MCMv3.1 and the different constrained cases to understand the model's prediction of RO_2 in relation to HO_x.

The predicted concentrations for RO_2 in the different modeling scenarios are shown in Fig. 5. The HO_x-constrained (not shown) and OH-constrained cases predict the same concentration of RO_2 because the effects of the OH constraint supersede any effects of the HO_2 constraint. The more direct coupling between OH and RO_2 radicals is also evident when comparing the HO_x-unconstrained and constrained cases: the higher concentrations of RO_2 from 10:00–16:00 in the unconstrained case are coincident with the model's overprediction of OH, noted previously and shown in Fig. 3.

The RO_2/HO_2 ratios (shown in Fig. 5b vs. NO) are another metric used to understand the prediction of RO_2 as it relates to HO_x. In each of the modeled scenarios in steady state, the RO_2/HO_2 ratio is between 0.7–1, whereas in the fully constrained case, the ratios are significantly lower and drop below 0.2 when NO>7 ppb. As mentioned previously, the coupling between OH and RO_2 is more direct than that between HO_2 and RO_2. As such, the lower-than-expected ratios are a direct result of the fixed OH concentration eliminating any effects that a fixed HO_2 concentration may have. In

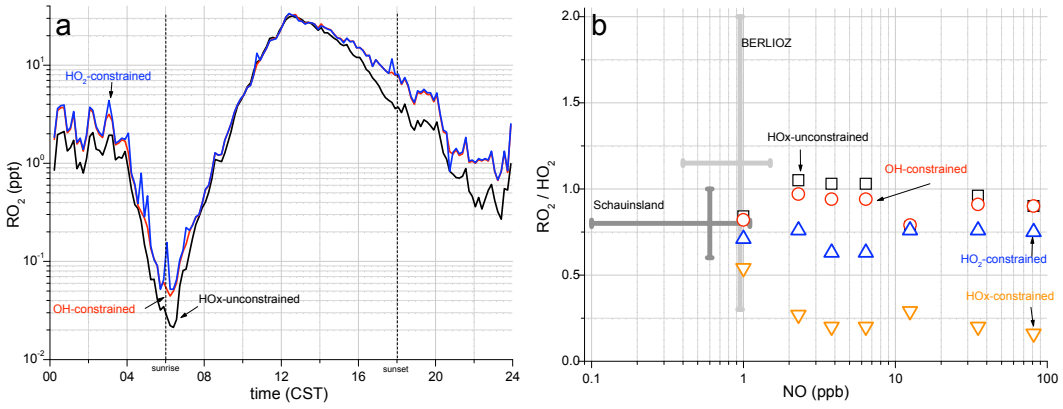

Fig. 5. Predicted RO_2 concentrations **(a)** and the ratio of RO_2/HO_2 vs. NO **(b)** for different modeling scenarios: HO_x-unconstrained (black line and squares), OH-constrained (red line and circles), and HO_2-constrained (blue line and triangles-up), and HO_x-constrained (orange triangles-down). The RO_2 concentration demonstrates an expected near-linear dependence on OH concentration. The steady-state models similarly predict RO_2/HO_2 ratios ∼1 at concentrations of NO ranging from 1–100+ ppb; however, the HO_x-constrained case predicts a much lower ratio, particularly at high NO (>7 ppb).

other words, with just a fixed HO_2 concentration, the profile of OH and the predicted concentrations are distorted (Fig. 3b) because of the fast HO_2+NO reaction (P4 in Fig. 1). However, in the HO_x-constrained model, the OH constraint offsets this forcing by HO_2 (which also yields an unbalanced model). We consider the predicted RO_2 concentration in the HO_x-constrained case as a lower limit.

3.5 Chain length

Chain length is broadly defined as the number of times that a hydroxyl radical will be regenerated via the RO_x cycle (Fig. 1). The radical chain length is a parameter that captures the characteristics of the fuel (i.e., VOC) in its oxidative environment. It is an effective means to assess the relative importance of new radical production relative to radical propagation in the MCMA. Strictly speaking, chain length is only a well defined quantity if the radical chain has a single point of initiation and a single point of radical termination (i.e., a linear radical chain reaction). Atmospheric RO_x cycling is inherently more complex: multiple reactions initiate the radical chain by providing sources for different radical intermediate species of the radical chain. Similarly, multiple reactions can terminate the radical chain at different RO_x radical intermediate species. To our knowledge there is currently no definition of chain length available in the literature that accounts for this atmospheric complexity. We define two parameters that both characterize chain length: n(OH) and ω. n(OH) is defined from a perspective of radical initiation, whereas ω is defined from a perspective of radical termination, i.e., treats radical propagation as a first order exponential decay process. Both parameters are quantitatively comparable, and each parameter is discussed in greater detail below.

We define n(OH), as:

$$n(\mathrm{OH}) = \gamma_{\mathrm{OH}} \left[\frac{\Sigma \mathrm{OH_{new}} + \text{propagated OH}}{\Sigma \mathrm{OH_{new}}} \right], \quad (1)$$

The γ_{OH} term is the fraction of OH entering the radical cycle:

$$\gamma_{\mathrm{OH}} = \frac{(\mathrm{OH} \rightarrow \mathrm{RO_2}) + (\mathrm{OH} \rightarrow \mathrm{HO_2})}{\text{total OH loss}}. \quad (2)$$

Total OH loss includes all pathways in which OH is permanently lost or has the potential to be recycled i.e., it is equal to the sum of all propagation (P1 and P5, Fig. 1) and termination routes (T1, Fig. 1).There are numerous parameters used to calculate chain length found in the literature (e.g.,Wagner et al. (2003); Seinfeld and Pandis (1998); Emmerson et al. (2007); Stroud et al. (2004); Martinez et al. (2003)). Most parameters for chain length assume that a single OH radical will cycle through at least once (i.e., n(OH)=1). If radical termination rates exceed propagation rates throughout the RO_x cycle, then we conclude that a single radical may not complete the cycle before being removed from the system. We have therefore added the γ_{OH} term. While this scenario (i.e., n(OH)<1) is unlikely in a polluted environment such as Mexico City, it is nonetheless an important adjustment to remain consistent in our calculation of n(OH) as a quantitative measure of chain length i.e., as the amplification of radical sources.

The $\Sigma \mathrm{OH_{new}}$ term is defined in Eq. (1) of Volkamer et al. (2010) and is the sum of all new RO_x radical production, weighted using conversion factors for the respective species into OH:

$$\gamma_{\mathrm{HO_2}} = \frac{\mathrm{HO_2} \rightarrow \mathrm{OH}}{\text{total } \mathrm{HO_2} \text{ loss}}, \quad (3)$$

$$\gamma_{\mathrm{RO}} = \frac{\mathrm{RO} \rightarrow \mathrm{HO_2}}{\text{total RO loss}}, \text{and} \quad (4)$$

$$\gamma_{RO_2} = \frac{RO_2 \rightarrow RO}{\text{total } RO_2 \text{ loss}}. \quad (5)$$

The ΣOH_{new} term is then defined as:

$$\Sigma OH_{new} = [OH]_{new} + \gamma_{HO_2} \cdot [HO_2]_{new} + \gamma_{HO_2} \cdot \gamma_{RO} \cdot \gamma_{RO_2} \cdot [RO_2]_{new}, \quad (6)$$

The calculation of n(OH) is most sensitive to the definition of initiation and propagation terms, and to a lesser degree termination. This requires careful accounting of the reactive pathways. The definitions employed here are similar to those used by Wagner et al. (2003):

- new radical production (i.e., initiation) is the breakdown of a closed shell molecule into two radicals or as the conversion of O_3 or NO_3 into a RO_x species;
- propagation is the transformation of one RO_x species into another;
- termination (i.e., radical sinks) is the formation of a closed shell molecule from the reaction of two radicals; and,
- the mechanism contains certain species that are in fast equilibrium with radicals, such as PAN. For these compounds, a net term is calculated. The net parameter is then appropriately classified as either production or termination.

In contrast to Wagner et al. (2003), we treat absolute fluxes for fast radical-radical reactions and HONO formation. Wagner et al. (2003) defined "delayed propagation" as fast radical-radical reactions form a radical reservoir that subsequently photolyzes to yield two radicals. Similarly, they define a net flux production of OH by subtracting the production of HONO (from the reaction between OH and NO) from the production of OH via HONO photolysis. This term is then lumped into ΣOH_{new}. We have assessed the effect of including a "delayed propagation" term in the calculation of n(OH). When including the net flux from radical-radical recombination reactions and the subsequent photolytic decomposition reactions for all the appropriate species (i.e., hydroperxide, organic peroxides, and oxygenated compounds e.g., aldehydes), we observe a modest increase in n(OH) (not shown); however, this is a function of accounting, and not a chemical manifestation of radical cycling. The differences are only observed during the day-time because OVOCs are formed from the processing of primary emissions at sunrise that make the greatest impact on the delayed propagation accounting. Wagner et al. (2003) uses a similar net flux approach in the treatment of HONO. A potential problem associated with using the net flux approach for HONO is a negative term in the summation of ΣOH_{new}. That is, whenever HONO formation is larger than HONO photolysis, the contribution of new OH to ΣOH_{new} may be a negative number, which does not make physical sense (see Volkamer et al. (2010) for more discussion). Furthermore, a correlation of production and loss terms creates a convolution that should be avoided to study radical cycling chemistry. Ultimately, our determination of n(OH) as a parameter for chain length does not include "delayed propagation" or a net flux approach for HONO accounting. In our case, the processes are treated rigorously as either termination or new radical production.

Having defined the various radical reaction pathways, we use the grouped terms to calculate n(OH). Rather than calculate a single OH chain length based solely on the "long" chain [L: OH→RO_2→RO→HO_2], we also consider the direct cycle between between OH and HO_2 i.e., the "short" chain (S). That is:

$$n(OH) = \gamma_{OH}\left[\alpha_{OH\rightarrow HO_2} n(OH)_S + \beta_{OH\rightarrow RO_2} n(OH)_L\right], \quad (7)$$

where

$$n(OH)_S = \frac{([OH]_{new} + \gamma_{HO_2} * [HO_2]_{new}) + (OH \rightarrow\ HO_2)}{[OH]_{new} + \gamma_{HO_2} * [HO_2]_{new}}, \quad (8)$$

$$n(OH)_L = \frac{\Sigma OH_{new} + (OH \rightarrow\ RO_2)}{\Sigma OH_{new}} \quad (9)$$

$$\alpha_{OH\rightarrow HO_2} = \frac{OH \rightarrow HO_2}{OH \rightarrow HO_2 + OH \rightarrow RO_2}, \text{and} \quad (10)$$

$$\beta_{OH\rightarrow RO_2} = 1 - \alpha_{OH\rightarrow HO_2}. \quad (11)$$

The median values for n(OH) and γ for both the HO_x-constrained and HO_x-unconstrained cases are shown in Fig. 6. In the HO_2- and HO_x-constrained cases, cycling is high in the morning, with a peak of 25 around 06:30 and then decreases to 15 over the next hour. From 10:30 to 14:30, n(OH) is between 3 and 5. Conversely, there is no morning peak evident in the HO_x-unconstrained case. This difference in n(OH) is coincident with previously noted missing reactivity shortly after sunrise and during rush-hour. The n(OH) for the HO_x-unconstrained model reaches a high value of about 4 around 05:00 and is in the range of 2.5–4 throughout the day. The peak difference in chain length values occurs at 05:30, at which time the median value for the constrained case is a factor of 9 higher than the unconstrained modeling.

The conversion factors, γ_{RO_x} shown in the upper panel of Fig. 6, provide a means to understand cycling and chain length via an alternative approach. The conversion factors are a measure of radical propagation efficiency relative to termination. We treat radical cycling as a first order exponential decay process in which the conversion efficiencies are related to the propagation of the OH radical. We define a parameter, ω, so that:

$$\gamma^{\omega}_{RO_x} \doteq \frac{1}{e}, \text{and} \quad (12)$$

$$\omega = -[\ln \gamma_{RO_x}]^{-1}, \text{where} \quad (13)$$

$$\gamma_{RO_x} = \gamma_{OH} \times \gamma_{RO_2} \times \gamma_{RO} \times \gamma_{HO_2} \quad (14)$$

The median ω value for the HO_x-constrained case is shown in Fig. 6. The chain length parameters have different perspectives with regard to radical cycling: the n(OH) focuses on propagation and initiation radical fluxes, while ω focuses on branching ratios for individual RO_x species to propagate versus terminate the radical chain. The agreement between n(OH) and ω is a measure of our understanding of radical cycling. In principle, the values for each should be the same; however, the plots for n(OH) and ω in both the HO_x- and HO_2-constrained cases show significant differences, particularly between 04:00–10:00, and again after 14:00.

In a straight radical chain, the condition of radical concentrations in steady state imposes the constraint that radical initiation and termination fluxes are equal. In atmospheric RO_x radical cycling it follows from Eqs. (1) and (13) that in order to bring n(OH) and ω into agreement, the HO_2 constrained model requires: 1) additional radical sources (i.e., lowers n(OH)); 2) an HO_2 sink and/or lower radical conversion efficiencies (i.e., lowers n(OH) and ω) or, 3) a combination of 1 and 2. Alternatively, a higher value of ω could reduce the mismatch between both metrics of radical cycling in the HO_2 constrained model. However, this would require higher gamma values (fewer radical sinks) and seems somewhat unlikely for the following reasons: during the period of most significant disagreement between ω and n(OH), the product of the γ-values varies between 0.6–0.7 (see upper panel of Fig. 6). In order for ω to reach a chain length of 20, for instance, the product of the γ-values must approach 0.95, which is inconsistent with our current understanding of organic peroxyl and hydroperoxyl radical kinetics. It should be noted that any increase in the radical conversion efficiencies of $RO_2 \rightarrow RO$, $RO \rightarrow HO_2$, and $HO_2 \rightarrow OH$ will have a non-linear effect on chain length calculation, as it will increase the contribution of new HO_2 and/or new RO_2 to the ΣOH_{new} term, and this lowers n(OH).

Assuming the HO_x measurements are correct, we conclude that there are two possible explanations to resolve the inconsistency between n(OH) and ω: 1) an additional RO_x radical source is needed, and 2) an additional HO_2 sink is required that does not form OH. Note, however, that both (1) and (2) are necessary in order for the chain length results to be consistent.

We have identified the following laboratory findings that may affect chain length:

– The photolysis of nitrylchloride ($ClNO_2$) as a source for RO_2 at high VOC concentrations (Roberts et al., 2008; Thornton et al., 2010). As discussed in Volkamer et al. (2010), this RO_2 source is likely operative and relevant in Mexico City.

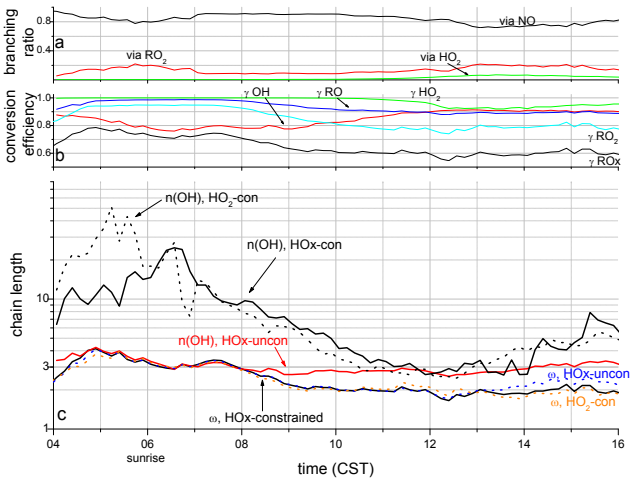

Fig. 6. Panel **(a)** at the top breaks down the branching ratios of $RO_2 \rightarrow RO$ radical reaction pathways via NO, RO_2, and HO_2 to demonstrate that the afternoon chemistry is still very much driven by NO_x and much less by organic peroxyl radicals formed as products of secondary oxidation. Panel **(b)** in the middle shows the conversion factors, γ, for the HO_x-constrained case. Panel **(c)** at the bottom shows the chain length parameters, n(OH) for the HOx-constrained (black line, solid), HO_x-unconstrained (red line), and HO_2-constrained (black line, dashed) scenarios and w for the HO_x-constrained (black line), HO_x-unconstrained (blue, dashed), and HO_2-constrained (orange, dashed) scenarios.

– The formation of OH and HONO from the reaction between $NO_2{}^*$ and water vapor as reported by Shuping et al. (2008). We introduced a series of reactions into the MCM to account for this reaction and no appreciable difference was observed in the chain length parameters.

– The formation of HNO_3 via reaction between HO_2 and NO in the presence of water vapor as reported by Butkovskaya et al. (2005) and Butkovskaya et al. (2007). The mechanism is consistent with the second explanation listed above; however, only introducing a HO_2 sink would increase missing reactivity in the model.

– The formation of OH from the reaction betwen organic peroxy radicals and HO_2 as reported by Hasson et al. (2004). We note that this mechanism is most significant at low levels of NO_x.

– Finally, the formation of OH from organic peroxy radicals as reported by Hatakeyama et al. (1986) and Peeters et al. (2009).

The first three (3) points would decrease chain length and the last two (2) points would increase chain length.

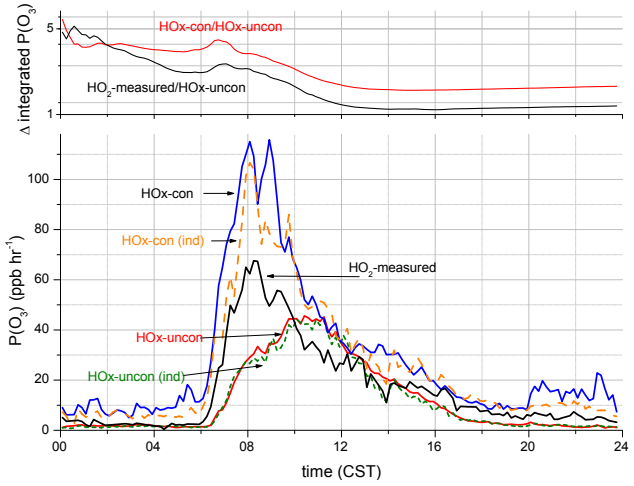

Fig. 7. The median diurnal profile for ozone production for individual day modeling is shown for the HO_x-constrained (orange line) and HO_x-unconstrained (green line), as well as for the median-model runs for HO_x-constrained (blue line) and HO_x-unconstrained (red line). Finally, $P(O_3)$ as calculated using only measured HO_2 is shown as the black line. The top panel results from dividing the integral of the median $P(O_3)_{HO_x\text{-con}}$ by the median $P(O_3)_{HO_x\text{-uncon}}$ (red line) and median $P(O_3)_{HO_2\text{-}con}$ by the median $P(O_3)_{HO_x\text{-uncon}}$ (black line).

3.6 Ozone production

Ozone formation is essentially a competition process between VOC and NO_x for OH (Seinfeld and Pandis, 1998). Net instantaneous ozone production, $P(O_3)$, is a measure of ozone formation as a result of NO oxidation via reaction with HO_2 or RO_2, yielding NO_2 and OH or RO, respectively. The production rate also accounts for radical loss channels forming HNO_3 and RNO_3. The net instantaneous O_3 production is calculated as:

$$P(O_3) = k_{HO_2+NO}[HO_2][NO] + \Sigma k_i[RO_2]_i[NO] - P(HNO_3) - P(RNO_3) \quad (15)$$

The median $P(O_3)$ diurnal profiles for the individual days and the median model in the HO_x-constrained and HO_x-unconstrained scenarios are shown in Fig. 7. The median profile of $P(O_3)$ as calculated using only measured HO_2 is also shown.

The median-model HO_x-constrained, median of individual day HO_x-constrained modeling, and HO_2-measured cases exhibit similar profiles for $P(O_3)$, with a peak at 08:00 of 115, 107, and 65 ppb hr^{-1}, respectively. The median-model HO_x-unconstrained and individual day HO_x-unconstrained modeling show similar profiles, but are very different from the other 3 cases shown. The timing of the peak ozone production is shifted by about 2 h, and shows a much less pronounced peak of 45 ppb hr^{-1}. We consider the profiles for both the HO_x-constrained cases as lower limits because of a lower-than-expected RO_2/HO_2 ratio, as shown in Fig. 5b. If a RO_2/HO_2 ratio of unity is assumed, the magnitude of $P(O_3)$ increases to well above 100 ppb hr^{-1}.

The differences observed in the $P(O_3)$ profiles, most notably between 06:00 and 10:00, are coincident with the aforementioned missing reactivity. The under-estimation of HO_x radicals in the unconstrained code manifests itself in both the magnitude and timing of peak ozone production. Despite the fact that the various profiles come into good agreement by 10:00, the measurements indicated that the bulk of $NO \rightarrow NO_2$ conversions take place before that time. The upper panel of Fig. 7 quantifies the effects of the missing reactivity on the oxidative capacity of the Mexico City atmosphere. The HO_x-constrained case predicts a minimum of 75% greater cumulative ozone production than the unconstrained case throughout the day, with a factor of 5 difference in the early morning at the onset of photochemical processing.

4 Comparison to other studies

4.1 Radical budgets

The MCMv3.1 has only recently been used in similar detail to quantify radical fluxes for initiation, propagation, and termination. In Part 1, Volkamer et al. (2010) compare new radical production rates in the MCMA to other airmasses, noting both the homogeneity of radical sources in the MCMA and the higher production rates. The radical fluxes for cycling routes that we report for both the HO_x-unconstrained and HO_x-constrained cases are considerably higher than those reported elsewhere (Emmerson et al., 2007, 2005; Platt et al., 2002). Apart from the $RO \rightarrow HO_2$ route, the radical flux from one RO_x radical to another is roughly 1.5–3 times larger in the MCMA compared to the cleaner sub-urban airmass observed during the TORCH campaign, and the semi-polluted atmosphere in Birmingham during the PUMA campaign. The radical flux of propagation pathways is higher for the MCMA due to higher NO_x concentrations and VOC concentrations, and higher rates of radical initiation. The $RO \rightarrow HO_2$ flux in the MCMA is comparable to the value reported for Birmingham for 2 reasons: 1) at the high concentrations of NO observed during MCMA-2003, the conversion efficiency for the $RO_2 \rightarrow RO$ route is lower because of the formation of organic nitrates (RNO_3). This yields fewer RO radicals, meaning a lower flux into HO_2. 2) We observe a much higher rate of thermal decomposition of RO radicals back into RO_2 radicals. A direct comparison with the BERLIOZ campaign is difficult because the radical production rates are distinguished only by production and destruction.

4.2 Missing HO_x radicals

The under-prediction of OH and HO_2 in our HO_x-unconstrained model has also been observed in other

environments, including atmospheric chamber studies (Bloss et al., 2005a,b), the upper troposphere (Folkins et al., 1997; Tan et al., 2001; Faloona et al., 2000), and other urban areas (Martinez et al., 2003; Ren et al., 2003). Shirley et al. (2006) employ the RACM mechanism to study the MCMA (2003 campaign) and do not observe the same missing radicals at high NO_x concentrations, and report that the measured-to-modeled ratios during rush hour for HO_2 is 1.5. Dusanter et al. (2009) use the same RACM mechanism, with different constraints, to study the MCMA (2006 campaign) and note an under-prediction of HO_2 in the morning (08:00–11:30), peaking at a factor of about 5 at 10:00. They offer three potential explanations, including (i) close emission sources of NO_x and VOC leading to inhomogeneous air masses, (ii) a missing radical source, and (iii) an over-estimated HO_2 to OH radical propagation route in the code due to an unknown chemical process that converts OH into peroxy radicals. Similarly, Ren et al. (2003) note an increasing measured-to-modeled ratio with increasing NO. At NO concentrations greater than 10 ppb, RACM under-predicts HO_2 by a factor of 2–20, similar to what we observe in the MCMA. To explain the difference, they suggest unknown HO_x sources that increase with NO, or shortcoming in HO_x-NO_x chemistry. Based on our analysis using the detailed MCMv3.1 and the chain length cycling parameters, n(OH) and ω, we conclude that there is a significant missing source for HO_2 and smaller one for OH. Because the predicted OH concentrations are generally very good, the introduction of a missing source for HO_2 must be accompanied by a pathway that does not form OH via reaction with NO (i.e., a sink for HO_2 radicals) or be accompanied by an efficient OH loss mechanism consistent with the discussion in Sect. 3.1.

The very high NO_x concentrations observed during MCMA-2003 makes our study unique amongst those employing the MCM and extends the NO_x range over which MCM has been employed in field studies. The median peak NO_x concentration employed here is about 130 ppb, with some days as high as 250 ppb. Our results demonstrate the incomplete understanding of HO_x chemical cycling at high NO_x beyond experimental doubt. In other studies employing the MCM, the peak NO_x concentrations are roughly 30 ppb for PUMA-summer, 30 ppb for BERLIOZ and 25 ppb for the TORCH campaign. High concentrations of NO_x were observed during the winter months of the PUMA campaign (140 ppb), however, HO_2 measurements were largely unavailable to compare with predicted values. As such, the noted missing radicals, while difficult to compare directly with other field campaign analyses employing the MCM, presents confirmation at previously unstudied high NO_x conditions. The key message from our work is that comparing radical concentrations is misleading when comparing models because it is not reflective of the radical fluxes and reactivites. This is overcome by using the two chain length parameters employed herewithin.

4.3 Defining a chain length parameter

The chain length parameter n(OH) is widely used as a quantitative measure of radical cycling, but the equations used to calculate the parameter vary significantly. We evaluate several of these equations here. Seinfeld and Pandis (1998) calculate it as:

$$n(\mathrm{OH})_{\mathrm{Seinfeld/Pandis}} = \frac{\text{new OH} + \text{old OH}}{\text{new OH}}, \quad (16)$$

where "old" OH is defined as recycled or propagated OH, a similar equation to the one employed here. On the other hand, in the TOPSE campaign, Stroud et al. (2004) calculate chain length as:

$$n(\mathrm{OH})_{\mathrm{TOPSE}} = \frac{P(\mathrm{OH})_{\mathrm{cycling}}}{L(\mathrm{RO_x})}, \quad (17)$$

where $P(\mathrm{OH})_{\mathrm{cycling}}$ is OH radical production from propagation routes (i.e., $HO_2 \rightarrow$OH) only and $L(\mathrm{RO_x})$ is the sum of all radical losses. In a slightly different approach, Emmerson et al. (2007) calculate chain length as:

$$n(\mathrm{OH})_{\mathrm{TORCH}} = \frac{P(\mathrm{OH})_{\mathrm{HO_2 \rightarrow OH}}}{\text{new OH}}, \quad (18)$$

where the OH production term is solely defined by the HO_2 propagation route and new OH is the same as I1 in Fig. 1.

As part of the Southern Oxidants Study (SOS), Martinez et al. (2003) use the following equation:

$$n(\mathrm{OH})_{\mathrm{SOS}} = \frac{[\mathrm{OH}] \cdot \mathrm{OH}_{\mathrm{reactivity}} - L(\mathrm{HO_x})}{L(\mathrm{HO_x})}, \quad (19)$$

The range of equations for OH radical chain length make comparisons between airmasses of different VOC and NO_x loadings extremely difficult. For instance, at peak NO_x concentrations around 07:00 we calculate a chain length using the equations defined above and get a range of 14–45. By 12:00, they come into better agreement, but the range of values is still 2–6. There is a need for a formalized equation to match the definition of chain length for sufficiently conclusive comparisons between airmasses.

In the case of the equation provided by Seinfeld and Pandis (1998), they do not account for the sink of OH radicals, as defined by us as $\gamma_{(\mathrm{OH})}$ in Sect. 3.5. Similarly, in applying their equation, we must assume that "new OH" is equivalent to $\Sigma \mathrm{OH}_{\mathrm{new}}$. In the TOPSE and SOS calculation of chain length, the role of new radical formation is folded entirely into radical propagation and termination. Ultimately, both of these assumptions over-simplify the conversion efficiency between RO_2 and HO_2 to OH. The TORCH calculation over-simplifies radical initiation. As mentioned previously, when accounting for "new OH", the sum of new radicals from other sources should be counted. This is particularly important because the sum of new RO_x radical production is considerably larger than new OH radical production (see Volkamer et al., 2010).

Each of the equations for chain length provides a quantitative determination of radical propagation relative to initiation and/or termination, yet they lack consistency. With MCM we can account for each of the radical initiation, propagation, and termination pathways (Fig. 1) and we make no assumptions about the VOC or NO_x environment. Our explicit calculation of OH chain length is a normalized calcuatlion that is linked to production rates and is a quantitative determination of the amplification of radical sources. We consider it a valuable tool in assessing the oxidative capacity of a given airmass and provides the quantitative rigor necessary to compare it to other airmasses.

4.4 Ozone production

Our comparison of ozone production to other studies focuses on magnitude and timing of ozone production. In terms of magnitude, we report similar values as those reported by Shirley et al. (2006) using RACM and by Lei et al. (2007) in a 3-D chemical transport study. Compared to other cities, we report much higher values of ozone production (Kleinman et al., 2005). The study by Ren et al. (2003), with underpredicted HO_2 concentrations in the model, observe a similar difference between $P(O_3)$ from measurements compared to the model as shown here in Fig. 7.

In terms of the timing, the measurements of OH, HO_2, NO, and NO_2 in the MCMA indicate a much different profile for ozone production than the model suggests. As shown in Fig. 7, the model clearly lacks the sharp peak around 08:00. Instead we observe a broad peak between 10:00–11:00, some 2 h after measurements suggest peak ozone production. Similarly, in the results presented by Shirley et al. (2006), peak ozone production is around 09:30, nearly 1.5 h later than expected. In the case presented by Lei et al. (2007) using a chemical transport model, they observe peak ozone production around 12:30 (W. Lei, personal communication, 2007) more than 4 h later than expected by observations. In the PMTACS-NY study, measurements indicate peak ozone production around 09:00. In addition to a consistent underprediction of ozone production by the model compared to measurements, models do not predict a distinct peak in ozone production in the early morning.

5 Conclusions

High radical recycling fluxes are largely responsible for the high photochemical activity in the MCMA compared to other urban environments. In this study we have provided a unique perspective on radical recycling as the quantitative amplification of radical initiation fluxes (Volkamer et al., 2010). We use MCMv3.1, in combination with measurements of OH, HO_2 and OH loss rate (Shirley et al., 2006) to identify shortcomings in our understanding of radical cycling under conditions of high VOC and NO_x loadings characteristic of the MCMA, and other polluted urban environments.

– We find excellent agreement between a lower-limit measured concentration and the modeled concentrations of OH using MCMv3.1, with a notable under-prediction around 06:00–07:00. We observe a significant underprediction of HO_2. These missing radicals are most notable when NO_x concentrations are high (25–130 ppb). Despite a good correlation using a linear regression analysis for measured and modeled HO_x, we caution against this metric as it is weighted towards times when HO_x values are high and NO_x concentrations are low. The metric may simulate apparently good agreement between the model and measurements and does not reflect photochemical activity (i.e., radical fluxes). Our analysis extends the range over which MCMv3.1 has been tested under real-world conditions towards higher NO_x.

– A significant imbalance is identified in the measurements of OH, HO_2 and OH loss rates (Shirley et al. (2006); see Supplemental Information). Notably, HO_2 measurements are characterized by a high signal-to-noise ratio and are typically regarded as the most reliable of the HO_x related measurements (W. H. Brune, personal communication, 2003). Due to the measurement imbalance we can not simultaneously constrain the model for OH and HO_2 measurements, and balance OH production and loss. This limits our ability to test predictions of OH and HO_2. However, it does not limit our assessment of chain length from any balanced model (either not constrained by HO_x observations, or constrained by OH or HO_2). We define chain length as the number of times that a hydroxyl radical will be regenerated via the RO_x cycle.

– Atmospheric RO_x cycling is inherently complex and calculations of chain length suffer from multiple points of radical initiation and termination. We find that the determination of chain length using equations found in the literature vary by a factor of 3 if applied to the MCMA-2003 data set. Any exact determination of chain length requires a single point of initiation and/or termination. We calculate two chain length parameters: The first parameter, n(OH), calculates chain length from the perspective of radical initiation (see Eq. 1). The production of RO_x radicals is expressed in terms of OH-equivalents i.e., the multiple points of initiation are compressed into a single parameter ΣOH_{new}. The ω parameter calculates chain length based on consideration of radical termination (see Eq. 11). The ω parameter accounts for the multiple points of termination and does not depend on radical initiation. To our knowledge these parameters represent the first systematic attempt to capture the complexity of the atmospheric RO_x radical cycle and

may help normalize future attempts to compare chain lengths between air masses.

– Both chain length parameters give comparable numbers for the HO_x unconstrained model case ($1<n(OH)\sim\omega<4$). However, we find $n(OH)>20$ during morning hours if the model is constrained for HO_2 observations. As expected, ω remains unaffected by the HO_2 constraint. The high values of $n(OH)$ are not compatible with our understanding of radical termination. If the HO_2 observations are correct, there is no single process that can resolve the mismatch between $n(OH)$ and ω in the HO_2-constrained scenario. An additional RO_x radical source in combination with an additional HO_2 sink that does not form OH directly may resolve this conundrum. Note that any combination of processes would bypass the OH radical as an intermediate.

– The model under predicts the observations of OH and HO_2 during morning hours. Our analysis demonstrates that at very high NO_x (100 ppb) our understanding of the sources and fate of RO_x radicals is incomplete. We conclude that in order to reconcile models with observations, a significant portion of the RO_x radical fluxes needs to follow essentially different reaction routes that may not involve the OH radical as an intermediate species. A significant RO_2 source could be tied to chlorine radicals in the MCMA (see discussion in Volkamer et al., 2010), though it appears that most of the needed RO_2 source is currently still unaccounted for.

– Control strategies for effective air quality management rely on the predictive capacity of models. The shortcomings in our ability to predict the RO_x radical cycle with confidence have implications for ozone formation and the formation of SOA. For instance, the ozone production rates reported in this study are much higher than those reported elsewhere. Based on our current understanding that HO_2 radicals propagate to convert NO into NO_2 as part of the ozone production process (at high NO), we find that the model under predicts the accumulated amount of ozone by at least a factor of 2 compared to the HO_2-constrained model. The uncertainty due to missing radicals in models may appear reduced in urban airshed models that employ lumped chemical codes which are optimized to a specific target question (e.g., predicting ozone). However, the uncertainty inherent to these chemistry modules proves difficult to parameterize over a wide range of VOC and NO_x conditions (Carter, 2004). For conditions typical of the VOC limited chemistry relevant in the MCMA the uncertainty in predicting ozone ranges between 10-40% (or several 10 ppb at peak ozone concentrations). This uncertainty is comparable to that from uncertain emission inventories and meteorology (Lei et al., 2007). Furthermore, the underestimation of oxidant fields poses an additional modeling challenge with predicting the rapid formation of large amounts of SOA observed in urban air (de Gouw et al., 2005; Volkamer et al., 2006; Kleinman et al., 2008).

– There is a need for further laboratory research and field work to improve our understanding of RO_x radical initiation and cycling. In particular, RO_2 radical concentrations are poorly constrained by observations. Our understanding would benefit from data sets that co-locate multiple instruments capable of measuring HO_x, RO_2, and first order OH loss at high NO, NO with high sensitivity and time resolution (i.e., 100 ppt detection limit with a second time resolution), an extensive library of time-resolved VOC concentrations, and heterogeneous radical processes. To our knowledge, no field campaign has captured all of these measurements, and some of these measurements will require instrument development.

Supplementary material related to this article is available online at: http://www.atmos-chem-phys.net/10/6993/2010/acp-10-6993-2010-supplement.pdf.

Acknowledgements. The authors would like to thank the entire MCMA-2003 team. In particular, we would like to thank W.H. Brune for detailed measurements of OH, HO_2 and OH-reactivity and helpful discussion related to these measurements. This work was supported by the National Science Foundation (ATM-0528227), the Department of Energy (DE-FG02-0563980), the Alliance for Global Sustainability (AGS), and the Comision Ambiental Metropolitana (CAM) of Mexico City. R. Volkamer acknowledges consecutive fellowships by the Henry & Camille Dreyfus Foundation and Alexander von Humboldt Foundation and funding support from a CAREER award by the National Science Foundation, award ATM-0847793. P. Sheehy is grateful to J.I. Steinfeld.

Edited by: C. E. Kolb

References

Abram, J. P., Creasey, D. J., Heard, D. E., Lee, J. D., and Pilling, M. J.: Hydroxyl radical and ozone measurements in England during the solar eclipse of 11 August 1999, Geophys. Res. Lett., 27, 3437–3440, 2000.

Bethel, H. L., Arey, J., and Atkinson, R.: Products of the OH radical-initiated reaction of 3-hexene-2,5-dione, Environ. Sci. Technol., 35, 4477–4480, 2001.

Bloss, C., Wagner, V., Bonzanini, A., Jenkin, M. E., Wirtz, K., Martin-Reviejo, M., and Pilling, M. J.: Evaluation of detailed aromatic mechanisms (MCMv3 and MCMv3.1) against environmental chamber data, Atmos. Chem. Phys., 5, 623–639, doi:10.5194/acp-5-623-2005, 2005a.

Bloss, C., Wagner, V., Jenkin, M. E., Volkamer, R., Bloss, W. J., Lee, J. D., Heard, D. E., Wirtz, K., Martin-Reviejo, M., Rea, G., Wenger, J. C., and Pilling, M. J.: Development of a detailed chemical mechanism (MCMv3.1) for the atmospheric oxidation of aromatic hydrocarbons, Atmos. Chem. Phys., 5, 641–664, doi:10.5194/acp-5-641-2005, 2005b.

Butkovskaya, N., Kukui, A., and Le Bras, G.: HNO_3 forming channel of the HO_2+NOreaction as a function of pressure and temperature in the ranges of 72-600 torr and 223–323 K, J. Phys. Chem. A, 111, 9047–9053, 2007.

Butkovskaya, N. I., Kukui, A., Pouvesle, N., and Le Bras, G.: Formation of nitric acid in the gas-phase HO_2+NO reaction: Effects of temperature and water vapor, J. Phys. Chem. A, 109, 6509–6520, 2005.

Carslaw, N., Creasey, D. J., Heard, D. E., Lewis, A. C., McQuaid, J. B., Pilling, M. J., Monks, P. S., Bandy, B. J., and Penkett, S. A.: Modeling OH, HO_2, and RO_2 radicals in the marine boundary layer 1. Model construction and comparison with field measurements, J. Geophys. Res.-Atmos., 104, 30241–30255, 1999.

Carter, W. P. L.: Environmental Chamber Studies of Ozone Formation Potentials of Volatile Organic Compounds, in: Proceedings of the NATO Advanced Research Workshop "Environmental Simulation Chambers: Application to Atmospheric Chemical Processes", NATO Sciences Series, IV. Earth and Environmental Sciences, Kluwer Academic Publishers, Zakopane, Poland, 2004.

Curtis, A. and Sweetenham, W.: FACSIMILE/CEKMAT user's manual, Tech. Rep. AERE Rep-R12805, Her Majesty's Stationery Office, 1987.

de Gouw, J. A., Middlebrook, A. M., Warneke, C., Goldan, P. D., Kuster, W. C., Roberts, J. M., Fehsenfeld, F. C., Worsnop, D. R., Canagaratna, M. R., Pszenny, A. A. P., Keene, W. C., Marchewka, M., Bertman, S. B., and Bates, T. S.: Budget of organic carbon in a polluted atmosphere: Results from the New England Air Quality Study in 2002, J. Geophys. Res.-Atmos., 110(22), D16305, doi:10.1029/2004JD005623, 2005.

Donahue, N. M., Robinson, A. L., Stanier, C. O., and Pandis, S. N.: Coupled partitioning, dilution, and chemical aging of semivolatile organics, Environ. Sci. Technol., 40, 2635–2643, 2006.

Dusanter, S., Vimal, D., Stevens, P. S., Volkamer, R., and Molina, L. T.: Measurements of OH and HO_2 concentrations during the MCMA-2006 field campaign – Part 1: Deployment of the Indiana University laser-induced fluorescence instrument, Atmos. Chem. Phys., 9, 1665–1685, doi:10.5194/acp-9-1665-2009, 2009.

Dzepina, K., Volkamer, R. M., Madronich, S., Tulet, P., Ulbrich, I. M., Zhang, Q., Cappa, C. D., Ziemann, P. J., and Jimenez, J. L.: Evaluation of recently-proposed secondary organic aerosol models for a case study in Mexico City, Atmos. Chem. Phys., 9, 5681–5709, doi:10.5194/acp-9-5681-2009, 2009.

Emmerson, K. M., Carslaw, N., Carpenter, L. J., Heard, D. E., Lee, J. D., and Pilling, M. J.: Urban atmospheric chemistry during the PUMA campaign 1: Comparison of modelled OH and HO_2 concentrations with measurements, J. Atmos. Chem., 52, 143–164, 2005.

Emmerson, K. M., Carslaw, N., Carslaw, D. C., Lee, J. D., McFiggans, G., Bloss, W. J., Gravestock, T., Heard, D. E., Hopkins, J., Ingham, T., Pilling, M. J., Smith, S. C., Jacob, M., and Monks, P. S.: Free radical modelling studies during the UK TORCH Campaign in Summer 2003, Atmos. Chem. Phys., 7, 167–181, doi:10.5194/acp-7-167-2007, 2007.

Faloona, I., Tan, D., Brune, W. H., Jaegle, L., Jacob, D. J., Kondo, Y., Koike, M., Chatfield, R., Pueschel, R., Ferry, G., Sachse, G., Vay, S., Anderson, B., Hannon, J., and Fuelberg, H.: Observations of HO_x and its relationship with NO_x in the upper troposphere during SONEX, J. Geophys. Res.-Atmos., 105, 3771–3783, 2000.

Folkins, I., Wennberg, P. O., Hanisco, T. F., Anderson, J. G., and Salawitch, R. J.: OH, HO_2, and NO in two biomass burning plumes: Sources of HOx and implications for ozone production, Geophys. Res. Lett., 24, 3185–3188, 1997.

George, L. A., Hard, T. M., and O'Brien, R. J.: Measurement of free radicals OH and HO_2 in Los Angeles smog, J. Geophys. Res.-Atmos., 104, 11643–11655, 1999.

Hasson, A. S., Tyndall, G. S., Orlando, and J. J.: A Product Yield Study of the Reaction of HO_2 Radicals with Ethyl Peroxy ($C_2H_5O_2$, Acetyl Peroxy ($CH_3C(O)O_2$), and Acetonyl Peroxy ($CH_3C(O)CH_2O_2$) Radicals., J. Phys. Chem. A, 108, 5979–5989, 2004.

Hatakeyama, S., Washida, N., and Akimoto, H.: Rate constants and mechanisms for the reaction of hydroxyl (OD) radicals with acetylene, propyne, and 2-butyne in air at 297±2 K, J. Phys. Chem., 90, 173–178, 1986.

Heard, D. E., Carpenter, L. J., Creasey, D. J., Hopkins, J. R., Lee, J. D., Lewis, A. C., Pilling, M. J., Seakins, P. W., Carslaw, N., and Emmerson, K. M.: High levels of the hydroxyl radical in the winter urban troposphere, Geophys. Res. Lett., 31, L18112, doi:10.1029/2004GL020544, 2004.

Jenkin, M. E., Saunders, S. M., and Pilling, M. J.: The tropospheric degradation of volatile organic compounds: A protocol for mechanism development, Atmos. Environ., 31, 81–104, 1997.

Kleinman, L. I., Springston, S. R., Daum, P. H., Lee, Y.-N., Nunnermacker, L. J., Senum, G. I., Wang, J., Weinstein-Lloyd, J., Alexander, M. L., Hubbe, J., Ortega, J., Canagaratna, M. R., and Jayne, J.: The time evolution of aerosol composition over the Mexico City plateau, Atmos. Chem. Phys., 8, 1559–1575, doi:10.5194/acp-8-1559-2008, 2008.

Kleinman, L. I., Daum, P. H., Lee, Y. N., Nunnermacker, L. J., Springston, S. R., Weinstein-Lloyd, J., and Rudolph, J.: A comparative study of ozone production in five U.S. metropolitan areas, J. Geophys. Res.-Atmos., 110, D02301, doi:10.1029/2004JD005096, 2005.

Lei, W., de Foy, B., Zavala, M., Volkamer, R., and Molina, L. T.: Characterizing ozone production in the Mexico City Metropolitan Area: a case study using a chemical transport model, Atmos. Chem. Phys., 7, 1347–1366, doi:10.5194/acp-7-1347-2007, 2007.

Lewis, A. C., Carslaw, N., Marriott, P. J., Kinghorn, R. M., Morrison, P., Lee, A. L., Bartle, K. D., and Pilling, M. J.: A larger pool of ozone-forming carbon compounds in urban atmospheres., Nature, 405, 778–781, 2000.

Martin, P., Tuazon, E. C., Aschmann, S. M., Arey, J., and Atkinson, R.: Formation and atmospheric reactions of 4,5-dihydro-2-methylfuran, J. Phys. Chem. A, 106, 11492–11501, 2002.

Martinez, M., Harder, H., Brune, W., Di Carlo, P., Williams, E., Hereid, D., Jobson, T., Kuster, W., Roberts, J., Trainer, D., and Geyer, A.: The behavior of the hydroxyl and hydroperoxyl rad-

icals during TexAQS2000. Abstract A12D-0174, in: AGU Fall Meeting, EOS Transactions, San Francisco CA, 2002.

Martinez, M., Harder, H., Kovacs, T. A., Simpas, J. B., Bassis, J., Lesher, R., Brune, W. H., Frost, G. J., Williams, E. J., Stroud, C. A., Jobson, B. T., Roberts, J. M., Hall, S. R., Shetter, R. E., Wert, B., Fried, A., Alicke, B., Stutz, J., Young, V. L., White, A. B., and Zamora, R. J.: OH and HO_2 concentrations, sources, and loss rates during the Southern Oxidants Study in Nashville, Tennessee, summer 1999, J. Geophys. Res.-Atmos., 108(D19), 4617, doi:10.1029/2003JD003551, 2003.

Molina, L. T., Kolb, C. E., de Foy, B., Lamb, B. K., Brune, W. H., Jimenez, J. L., Ramos-Villegas, R., Sarmiento, J., Paramo-Figueroa, V. H., Cardenas, B., Gutierrez-Avedoy, V., and Molina, M. J.: Air quality in North America's most populous city overview of the MCMA-2003 campaign, Atmos. Chem. Phys., 7, 2447–2473, doi:10.5194/acp-7-2447-2007, 2007.

Olariu, R. I.: Atmospheric Oxidation of Selected Aromatic Hydrocarbons, Doctoral dissertation, Bergische Universitaet Gesamthochschule Wuppertal, 2001.

Olariu, R. I., Barnes, I., Becker, K. H., and Klotz, B.: Rate coefficients for the gas-phase reaction of OH radicals with selected dihydroxybenzenes and benzoquinones, Int. J. Chem. Kinet., 32, 696–702, 2000.

Peeters, J., Nguyen, T., and Vereecken, L.: HOx radical regeneration in the oxidation of isoprene, Phys. Chem. Chem. Phys., 11, 5935–5939, doi:10.1039/b908511d, 2009.

Platt, U., Alicke, B., Dubois, R., Geyer, A., Hofzumahaus, A., Holland, F., Martinez, M., Mihelcic, D., Klupfel, T., Lohrmann, B., Patz, W., Perner, D., Rohrer, F., Schafer, J., and Stutz, J.: Free radicals and fast photochemistry during BERLIOZ, J. Atmos. Chem., 42, 359–394, 2002.

Ren, X. R., Harder, H., Martinez, M., Lesher, R. L., Oliger, A., Shirley, T., Adams, J., Simpas, J. B., and Brune, W. H.: HO_x concentrations and OH reactivity observations in New York City during PMTACS-NY2001, Atmos. Environ., 37, 3627–3637, 2003.

Roberts, J. M., Osthoff, H. D., Brown, S. S., and Ravishankara, A. R.: N_2O_5 Oxidizes Chloride to Cl_2 in Acidic Atmospheric Aerosol., Science, 321, 1059, doi:10.1126/science.1158777, 2008.

Robinson, A. L., Donahue, N. M., Shrivastava, M. K., Weitkamp, E. A., Sage, A. M., Grieshop, A. P., Lane, T. E., Pierce, J. R., and Pandis, S. N.: Rethinking organic aerosols: Semivolatile emissions and photochemical aging, Science, 315, 1259–1262, 2007.

Salcedo, D., Onasch, T. B., Dzepina, K., Canagaratna, M. R., Zhang, Q., Huffman, J. A., DeCarlo, P. F., Jayne, J. T., Mortimer, P., Worsnop, D. R., Kolb, C. E., Johnson, K. S., Zuberi, B., Marr, L. C., Volkamer, R., Molina, L. T., Molina, M. J., Cardenas, B., Bernab, R. M., Márquez, C., Gaffney, J. S., Marley, N. A., Laskin, A., Shutthanandan, V., Xie, Y., Brune, W., Lesher, R., Shirley, T., and Jimenez, J. L.: Characterization of ambient aerosols in Mexico City during the MCMA-2003 campaign with Aerosol Mass Spectrometry: results from the CENICA Supersite, Atmos. Chem. Phys., 6, 925–946, doi:10.5194/acp-6-925-2006, 2006.

Saunders, S. M., Jenkin, M. E., Derwent, R. G., and Pilling, M. J.: Protocol for the development of the Master Chemical Mechanism, MCM v3 (Part A): tropospheric degradation of non-aromatic volatile organic compounds, Atmos. Chem. Phys., 3, 161–180, doi:10.5194/acp-3-161-2003, 2003.

Seinfeld, J. H. and Pandis, S. N.: Atmospheric Chemistry and Physics : From Air Pollution to Climate Change, Wiley, New York, 1998.

Shirley, T. R., Brune, W. H., Ren, X., Mao, J., Lesher, R., Cardenas, B., Volkamer, R., Molina, L. T., Molina, M. J., Lamb, B., Velasco, E., Jobson, T., and Alexander, M.: Atmospheric oxidation in the Mexico City Metropolitan Area (MCMA) during April 2003, Atmos. Chem. Phys., 6, 2753–2765, doi:10.5194/acp-6-2753-2006, 2006.

Shuping, L., Matthews, J., and Sinha, A.: Atmospheric Hydroxyl Radical Production from Electronically Excited NO_2 and H_2O, Science, 319, 1657–1660, 2008.

Stroud, C., Madronich, S., Atlas, E., Cantrell, C., Fried, A., Wert, B., Ridley, B., Eisele, F., Mauldin, L., Shetter, R., Lefer, B., Flocke, F., Weinheimer, A., Coffey, M., Heikes, B., Talbot, R., and Blake, D.: Photochemistry in the arctic free troposphere: Ozone budget and its dependence on nitrogen oxides and the production rate of free radicals, J. Atmos. Chem., 47, 107–138, 2004.

Tan, D., Faloona, I., Simpas, J. B., Brune, W., Olson, J., Crawford, J., Avery, M., Sachse, G., Vay, S., Sandholm, S., Guan, H. W., Vaughn, T., Mastromarino, J., Heikes, B., Snow, J., Podolske, J., and Singh, H.: OH and HO_2 in the tropical Pacific: Results from PEM-Tropics B, J. Geophys. Res.-Atmos., 106, 32667–32681, 2001.

Thornton, J., Kercher, J., Riedel, T., Wagner, N., Cozic, J., Holloway, J., Dubey, W., Wolfe, G., Quinn, P., Middlebrook, A., Alexander, B., and Brown, S.: A large atomic chlorine source inferred from mid-continental reactive nitrogen chemistry, 464, Nature, 271–274, doi:10.1038/nature08905, 2010.

Volkamer, R., Platt, U., and Wirtz, K.: Primary and secondary glyoxal formation from aromatics: Experimental evidence for the bicycloalkyl-radical pathway from benzene, toluene, and p-xylene, J. Phys. Chem. A, 105, 7865–7874, 2001.

Volkamer, R., Klotz, B., Barnes, I., Imamura, T., Wirtz, K., Washida, N., Becker, K. H., and Platt, U.: OH-initiated oxidation of benzene - Part I. Phenol formation under atmospheric conditions, Phys. Chem. Chem. Phys., 4, 1598–1610, 2002.

Volkamer, R., Molina, L., Molina, M., Shirley, T., and Brune, W. H.: DOAS measurement of glyoxal as an indicator for fast VOC chemistry in urban air, Geophys. Res. Lett., 32, L08806, doi:10.1029/2005GL022616, 2005.

Volkamer, R., Jimenez, J. L., San Martini, F., Dzepina, K., Zhang, Q., Salcedo, D., Molina, L. T., Worsnop, D. R., and Molina, M. J.: Secondary organic aerosol formation from anthropogenic air pollution: Rapid and higher than expected, Geophys. Res. Lett., 33(4), L17811, doi:10.1029/2006GL026899, 2006.

Volkamer, R., Sheehy, P., Molina, L. T., and Molina, M. J.: Oxidative capacity of the Mexico City atmosphere – Part 1: A radical source perspective, Atmos. Chem. Phys., 10, 6969–6991, doi:10.5194/acp-10-6969-2010, 2010.

Wagner, V., Jenkin, M. E., Saunders, S. M., Stanton, J., Wirtz, K, and Pilling, M. J.: Modelling of the photooxidation of toluene: conceptual ideas for validating detailed mechanisms, Atmos. Chem. Phys., 3, 89–106, doi:10.5194/acp-3-89-2003, 2003.

Wall, K. J., Schiller, C. L., and Harris, G. W.: Measurements of the HONO photodissociation constant, J. Atmos. Chem., 55, 31–54, 2006.